Electrocatalysis
DOI 10.1007/s12678-015-0253-2

ORIGINAL RESEARCH

Combinatorial Plasma Sputtering of Pt_xPd_y Thin Film Electrocatalysts for Aqueous SO_2 Electro-oxidation

A. Falch[1] · **V. Lates**[1] · **R. J. Kriek**[1]

Abstract A combinatorial sputtering system, based on magnetron enhanced plasma sputtering, was employed in the syntheses of Pt_xPd_y thin film catalysts, and a multi-channel potentiostat allowed for high-throughput parallel screening of the deposited electrocatalysts towards the electro-oxidation of aqueous sulphur dioxide (SO_2). Employing onset potential as the screening criterion, it was found that three Pt_xPd_y bimetallic combinations exhibited satisfactory performance with the best compositions being that of Pt_3Pd_2 and $PtPd_4$. Both these combinations exhibited the same lower onset potential of 0.587±0.004 V, SHE compared to that of pure Pt (0.598±0.011 V, SHE), and in addition contain less Pt in achieving these onset potentials.

Keywords Combinatorial sputtering · Sulphur dioxide · Electro-oxidation

Introduction

The hybrid sulphur cycle (HyS cycle), proposed by the Westinghouse Corporation [1], has received a fair amount of attention as a thermo-chemical water splitting cycle [2–4]. Sulphuric acid is thermally decomposed to produce aqueous sulphur dioxide (reaction 1), which is fed to a sulphur depolarised electrolyser (SDE) and electro-oxidised at the anode to again produce sulphuric acid as well as hydrogen ions (reaction 2). The hydrogen ions migrate through the membrane of the electrolyser to the cathode where it is reduced to hydrogen gas (reaction 3), while the electrochemically produced sulphuric acid is recirculated back to the decomposition reactor. The net SDE reaction therefore involves the conversion of aqueous sulphur dioxide into sulphuric acid and hydrogen gas (reaction 4), while the net HyS cycle reaction is that of water being split into hydrogen and oxygen (reaction 5):

$$H_2SO_4 \rightarrow SO_2 + H_2O + 1/2O_2 \quad (1)$$

$$SO_2 + 2H_2O \rightarrow H_2SO_4 + 2H^+ + 2e^- \quad (E^\circ = 0.17\ V, SHE) \quad (2)$$

$$2H^+ + 2e^- \rightarrow H_2 \quad (3)$$

$$SO_2 + 2H_2O \rightarrow H_2SO_4 + H_2 \quad \text{(net SDE reaction)} \quad (4)$$

$$H_2O \rightarrow H_2 + 1/2O_2 \quad \text{(net HyS Cycle reaction)} \quad (5)$$

Interest in the HyS cycle results from the fact that, whereas the anodic reaction for regular water electrolysis (reaction 6) occurs at a standard potential of 1.23 V, SHE [5], the anodic reaction for the SDE (reaction 2) occurs at a standard potential of 0.17 V, SHE [6], which translates into an energy gain of more than 1 V.

$$H_2O \rightarrow 1/2O_2 + 2H^+ + 2e^- \quad (E^\circ = 1.23\ V, SHE) \quad (6)$$

The possibility, however, exists for the SDE to be employed as a SO_2 sink, whereby SO_2 together with water is used as feedstock to convert an environmental pollutant into useable commodities, i.e. sulphuric acid and hydrogen gas. In contrast to regular water electrolysis systems, the SDE runs at a lower cell voltage and some of the electrical energy input is 'returned' in the form of an energy carrier, i.e. hydrogen gas, which translates into a substantial economic benefit [7].

For the SDE, an operational target has been set of 500 mA cm^{-2} at a cell potential of approximately 0.6 V [8]. This target can only be achieved through the development of an effective electrocatalyst for the anodic electro-oxidation of SO_2, and to that regard, the properties of the anode is regarded as pivotal for improving the entire HyS process [4]. While

✉ R. J. Kriek
cobus.kriek@nwu.ac.za

[1] Electrochemistry for Energy & Environment Group, Research Focus Area: Chemical Resource Beneficiation (CRB), North-West University, Private Bag X6001, Potchefstroom 2520, South Africa

Published online: 08 April 2015

platinum is still considered the standard anode catalyst for the SDE, several studies have been conducted on the subject, which amongst others include those listed in Table 1. As is the case with the oxygen reduction reaction in a fuel cell, efforts are underway to find an electrocatalyst other than platinum. Operating at about 100 °C and high sulphuric acid concentration, the anode electrocatalyst has to be not only active but must also be able to withstand this harsh environment. In an effort to reduce platinum content, it could be alloyed with either a more cost-effective noble metal or base metals. Although results obtained for platinum alloyed with non-noble metals show good activity [3], platinum alloyed with noble metals shows similar to or even higher activity than that of pure platinum. However, studies on this subject are limited [4].

The need therefore exists to research and develop new as well as improved catalysts for the electro-oxidation of SO_2 [12, 13]. A fast and effective means of achieving this is by employing high-throughput combinatorial screening [13–16], which is a technique that has gained a lot of interest over recent years. One of the very first remarks, with regards to multiple-sample syntheses and testing, was made by Hanak in 1970 who emphasised the fact that the search for new materials suffers due to the fact that handling one sample at a time, in the process of synthesis and chemical testing, is an expensive and time-consuming approach, which prevents the researcher to take full advantage of his/her talents and keeps the level of progress low [17]. He suggested the abandonment of the tedious efforts of single sample synthesis and testing, and the adoption of methods to process multiple materials simultaneously. As the need to explore efficient and systematic means of searching for alternative binary, ternary and higher materials grew, the field of combinatorial science gained interest [13, 18–22]. Some of the techniques that have been applied to a combinatorial approach include (i) sputtering [23], (ii) evaporation and molecular beam epitaxy [24], and (iii) pulsed laser deposition [25], either employing a form of the composition spread technique [17, 23] or using a discrete composition approach [18, 20]. It has to be stressed, however, that a high-throughput approach does not always allow for highly accurate and precise experimentation compared to conventional experimentation [12, 26]. It is aimed rather at investigating observable trends in the material of interest, such as catalytic activity for example, subsequent to which the initial observation is confirmed and optimised with more precise kinetic data [13]. One of the first examples of combinatorial electrochemistry involved generating a 645-member electrode array of Pt, Ru, Os, Ir and Rh employing a modified inkjet printer with metal salt 'inks' and subsequently screening the catalysts for methanol oxidation [27]. Numerous studies have followed where electrocatalysts have been investigated for a number of chemical reactions [28–30]; however, little research has been conducted on high-throughput combinatorial electrocatalyst development for SO_2 electro-oxidation as part of the HyS cycle.

Table 1 Studies on the catalyst of the anode as a means of improving the electrolysis performance of the HyS process

Year	Catalyst	Ref.
1973	Al-V mixed oxides with traces of Pt	[9]
1980	Pt, Pd, Au, Ru, Re, Ir and Rh	[10]
2007	Pt/C and Pd/C	[11]
2010	Pt-M/C (M=Co, Cr, Fe, Ru, Ir)	[3]
2012	Pt and Au	[2]
2014	Pt-M/XC72R (M=Pd, Rh, Ru, Ir and Cr)	[4]

In this study, we describe the high-throughput syntheses and screening of Pt_xPd_y thin films for the electro-oxidation of SO_2. Palladium was chosen to 'alloy' with platinum as some experimental studies [10, 31] as well as a theoretical molecular modelling study [32] pointed towards palladium being potentially more active than platinum for the electro-oxidation of aqueous SO_2. The thin films are obtained employing a vacuum sputtering system for the physical deposition of a discrete composition library with the dimensions of each pad being 3 mm×3 mm. This is followed by simultaneous electrochemical screening of the thin films by employing a specially designed electrochemical cell connected to a multi-channel potentiostat. With this multi-channel potentiostat, a rapid electro-analytical technique is applied to all synthesised materials as it does not require calibration and it is independent of the composition of the tested materials. The thin films (Pt_xPd_y combinations) were furthermore characterised by scanning electron microscopy (SEM) and energy-dispersive X-ray spectroscopy (EDX). Their activities are compared to the activity of pure sputtered Pt towards the oxidation of aqueous SO_2 using onset potential as the evaluative criterion.

Experimental Approach

Photolitography

Photolitography is employed to microfabricate a Ti-Au electrical circuit onto a SiO_2 wafer (Microchemicals, Germany), adapted from Strasser et al. [13] and Warren et al. [33]. The wafer has a diameter of 100 mm, with a thickness of 500–550 μm and consists of two semi-standard flats with an orientation of (100). A thin, uniform, 10-μm-thick layer of positive photoresist (PL177, Microchemicals) is put down onto the wafer by controlled addition of the photoresist (Performus dispensing system, EFD Nordson) and spin coating (Spin 150, SPS Ltd.) subsequent to which the wafer is dried at 80 °C for 15 min. The image mask of the circuit pattern is accurately fitted onto the wafer and the exposed ink is

developed by exposure to 5 mW/cm^2 UV light for 1 min in a UV box (Pluvex 1410, Mega Electronics, UK). The wafer is then placed in a developer solution (RS Universal developer) for 20 s and subsequently rinsed with water and dried with N_2. The size of the contact pad, onto which the thin film will be deposited, is 0.09 cm^2 with 2.5-mm spacing, and the size of the pin pad, which connects the individual contact pad to the potentiostat, is 2.5×6 mm with 1–1.5-mm spacing. Subsequent to development, the wafer is ready for deposition of the circuit by DC-magnetron vacuum sputtering. A 106.8-nm-thick Ti-Au layer (calibration of Ti and Au is done as described in the "Calibration of Sputtering Rate" section) is deposited onto the patterned wafer, employing the aperture as depicted in Fig. 2a, which allows the Ti and Au to deposit on the entire wafer.

The conditions for sputtering the circuit are as follows: vacuum base pressure of 5×10^{-7} Torr, chamber pressure of 8 mTorr, argon gas flow rate of 0.015 L min^{-1}, Ti DC power of 50 W for 235 s, and on top of the Ti layer a Au layer, DC power of 50 W for 280 s. The negative part of the circuit pattern is then stripped off so as to remove the sputtered metal from the black sections. This is done by placing the wafer in acetone and bubbling N_2 to impose agitation so as to speed up the process of stripping. The wafer is again covered with a layer of photoresist, where after only the contact pads and pin pads are developed by exposure to UV light for 1 min followed by 20 s in the developer. In order to confirm that the lines are insulated, each contact pad, line and pin pad combination of the circuit is scrutinised and tested employing a digital multimeter. This insulation step ensures that each contact pad, line and pin pad combination is insulated from all other combinations and to ensure that only the pads are exposed for electrochemical testing.

Combinatorial Deposition System

The combinatorial deposition system (Fig. 1) used for vacuum sputtering was custom-designed and supplied by PVD Products, USA.

The system is a sputter down setup with four water-cooled magnetron guns (Fig. 1a) hosting one target/metal disk each. The target diameter and thickness are fixed to 38.1 and 3.2 mm respectively and were obtained from ACI Alloys (Inc), California. The magnetron guns hosting the targets are focussed onto the aperture (Figs. 1b and 2a–d) of choice, and the target to substrate distance is constant at 90 mm. A computer-controlled shutter allows for the opening and closing of the target. Various holders and apertures (Fig. 2) were customised to allow for the following alternatives of sputtering: (a) on a 100-mm-diameter SiO_2 wafer (see holder in Fig. 2f) and on 16 glassy carbon (GC) electrodes (see holder in Fig. 2e), (b) on 4 GC electrodes at a time, (c) on only one square contact pad among a maximum of 64 electrode pads on the SiO_2 wafer, and (d) on only one circular GC electrode.

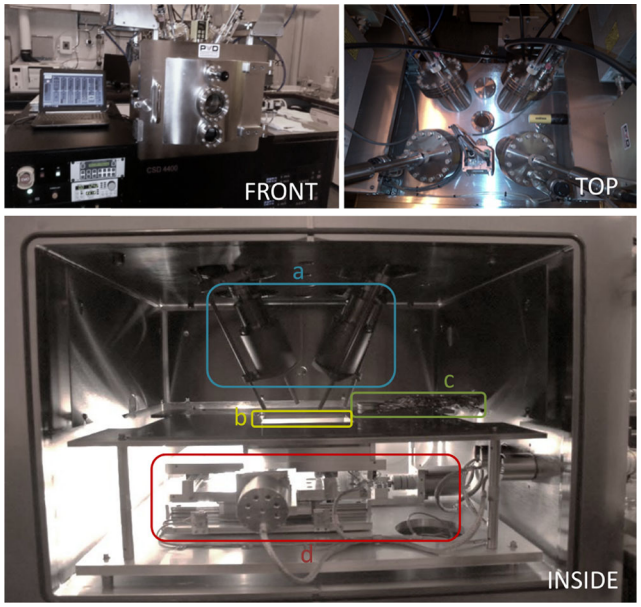

Fig. 1 Different views of the combinatorial deposition system. **a** Four downward facing magnetron guns, **b** variable aperture, **c** quartz crystal microbalance (QCM), and **d** programmable x-y stage

Prior to sputtering, the sputtering chamber is 'pumped down' to a base pressure of ~5×10^{-7} Torr using a rough pump (≥250 mTorr) and turbo pump (<250 mTorr) combination. The maximum power of the four direct current (DC) magnetron guns is 100 W, and two of these can switch to radio frequency (RF) mode when required (for example sputtering non-conductive targets, i.e. oxides) with a maximum power of 100 W. The programmable parameters that determine the composition and thickness of the sputtered films include the deposition time, regulated by the position of the shutter (open or closed) or by the on-off state of the magnetron, the power of the magnetron, and the argon pressure and flow rate. Calibration (refer to the "Calibration of Sputtering Rate" section for details) of each target, taking these parameters into consideration, was conducted by employing the built-in quartz crystal microbalance (QCM, Fig. 1c), which measures the change in the mass deposited per unit area as a change in frequency of a quartz crystal resonator.

Deposition of Thin Film Catalysts

The library of thin films is deposited one-by-one in a predefined sequence during which the sputtering parameters, derived from the calibration data, are specified in such a way so as to obtain a gradient of discrete compositions across the library. In this work, different molar ratio combinations of Pt and Pd were produced by simultaneously sputtering (co-depositing) the individual metals to obtain bimetallic materials. The different combinations were compared to pure Pt

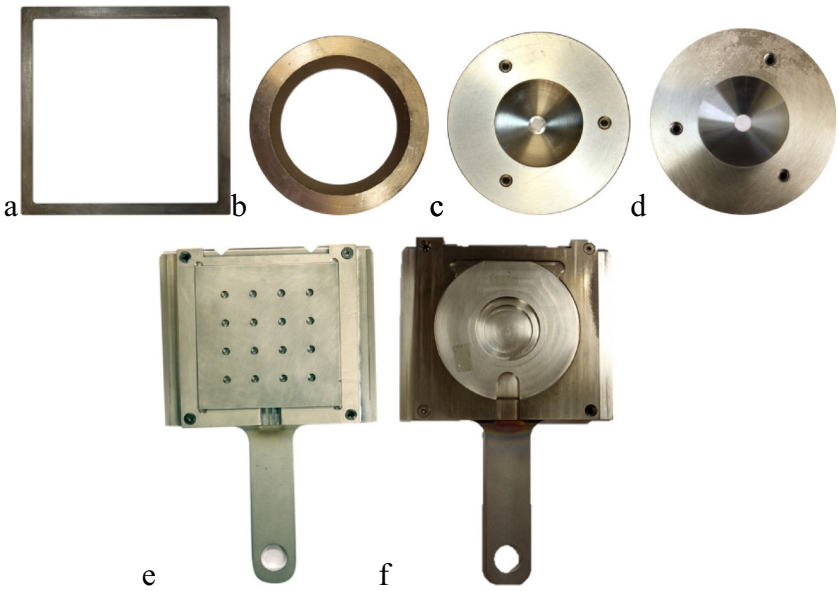

Fig. 2 Various apertures for sputtering on **a** a 100-mm-diameter SiO_2 wafer and 16 glassy carbon (GC) electrodes, **b** on 4 of 16 glassy carbon (GC) electrodes at a time, **c** only on one electrode among the 64 electrodes of the SiO_2 wafer, and **d** only on one GC electrode. Images **e** and **f** are holders for 16 GC electrodes and a SiO_2 wafer respectively which is placed on the programmable x-y stage

and Pd towards the oxidation of aqueous SO_2. Random positions were chosen for each Pt_xPd_y ratio (in triplicate) so as to validate whether the position of a specific electrocatalyst does not influence the electrical signal (performance) of the catalyst as the length of the contact lines do vary. To that regard, the contact pads that were not sputtered with Pt and Pd consisted of Au (the sputtered circuit). The programmable parameters that determine the composition and thickness of the sputtered films are listed in Table 2.

Physical Characterisation

Catalyst ratios were investigated non-destructively with reduced area analysis by employing SEM with an integrated XMax 20 EDX system (Oxford Instruments). Prior to determining catalyst ratios, mapping was performed (SEM with an integrated XMax 20 EDX system) to validate homogeneous sputtering. The whole wafer was fitted into the microscope chamber and the catalyst compositions were measured sequentially. Subsequent to the electrochemical investigation, the wafer, containing the circuit and thin film catalysts, was cut to obtain a cross section view using scanning electron microscopy (FEI Quanta FEG 250), which allowed the measurement and validation of film thickness.

Table 2 Power and time of deposition used for the syntheses of sputtered films with variable molar composition (Pt_xPd_y) and fixed thickness (40 nm)

Composition		DC power (Watt)		Time (s)
Pt	Pd	Pt	Pd	
0	1.0	0	50	150
0.1	0.9	17	90	74
0.2	0.8	24	60	99
0.4	0.6	62	60	74
0.6	0.4	50	22	138
0.8	0.2	85	15	106
1.0	0	50	0	226

Base pressure, 5×10^{-7} Torr; chamber pressure, 8 mTorr, argon flow rate, 0.015 L min^{-1}

Electrochemical Characterisation

Solutions for Electrochemical Measurements

In order to ensure that the electrocatalysts are all in the same electrochemical condition, preconditioning (see the "Electrochemical Measurements on the Wafer" section) was conducted in degassed (N_2 bubbled for 20 min) 0.1 mol L^{-1} $HClO_4$ (Merck). A 1 mol L^{-1} H_2SO_4 acid solution (pH=0.55) was made up by dilution of 95 wt% H_2SO_4 (Merck). This solution was degassed with N_2 for 15 min prior to linear polarisation. A stock solution of 1 mol L^{-1} Na_2SO_3 (Sigma Aldrich) was used as an in situ SO_2 source (reaction 7).

$$Na_2SO_3 + H_2SO_4 \rightarrow Na_2SO_4 + H_2O + SO_2 \quad (7)$$

All experiments were conducted in a water-jacketed electrochemical cell (300 mL) with the temperature (25 °C) controlled through an external circulation water bath (Julabo F12 ED). In all instances, Milli-Q water (Millipore Milli-Q ultrapure water system; 18.2 MΩ cm) was used.

Combinatorial Electrochemical Cell

Electrochemical testing was conducted employing a specially designed electrochemical cell (Fig. 3), which has been adapted

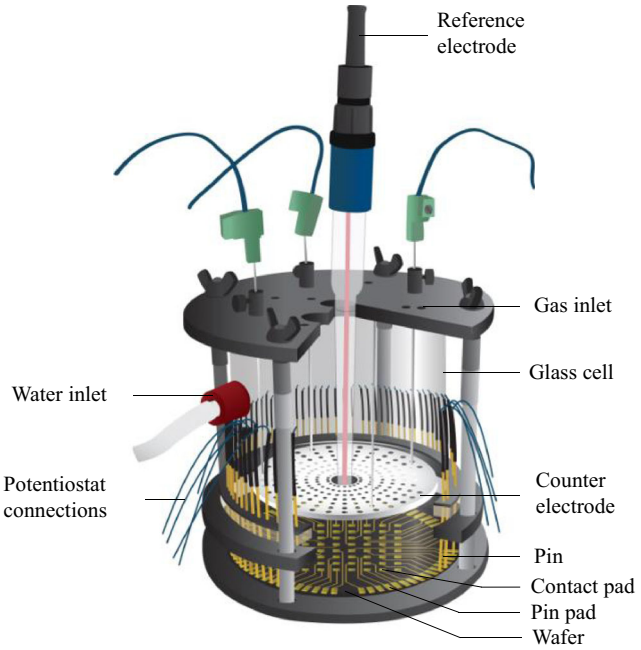

Fig. 3 A cutaway schematic drawing of the designed electrochemical cell (adapted from [34])

from the cell reported by Cooper et al. [34]. The wafer containing the sputtered electrocatalysts was placed at the bottom of the cylindrical double-wall glass cell body such that they were facing upward so as to be exposed to the electrolyte solution. The electrocatalysts and electrolyte were sealed off from the pin pads by an O-ring seal incorporated into the bottom wall of the bottomless cylindrical double-wall glass cell body. A Pt-plated Ti mesh electrode with a 7-cm diameter was placed parallel to the wafer at a distance of about 2.5 cm and served as a common counter electrode. A saturated calomel electrode (SCE, Radiometer Analytical REF 421) was used as the reference electrode and was placed above the working electrode array, protruding through an opening in the middle of the counter electrode. The distance between the capillary tip of the reference electrode and the working electrode pads at the centre and at the edge of the array ranged from about 1.5 to 2 cm. This distance was chosen so as to minimise the differences in the uncompensated ohmic resistance between the electrocatalysts. Voltage drops across the electrolyte between the reference electrode tip and individual working electrode pads were considered negligible [13] given the conductivity of the electrolyte and the magnitude of the measured currents.

Electrochemical Measurements on the Wafer

All electrochemical measurements were performed simultaneously with a 64-channel potentiostat (Arbin Instruments). The electrode preconditioning procedure involved, as a first step, conducting cyclic voltammetry (CV) scans between 1.441 V versus SHE to 0.041 V versus SHE starting at E_{ocp} (open circuit potential) for 25 cycles employing a scan rate of 50 mV s^{-1}. This was followed up with three CV scan cycles changing the anodic potential to 1.741 V versus SHE and finally the first step was repeated but only for three cycles. This preconditioning procedure is necessary to ensure obtaining repeatable results for subsequent linear polarisation scans (for SO_2 electro-oxidation). Linear polarisation runs (E_{low}=0.2 V vs SHE to 1.441 V vs SHE, based on the results of O'Brien et al. [35]) in the SO_2-containing solution were conducted at a scan rate of 10 mV s^{-1}. Electrodes were, however, not held at the E_{low} potential for 2 min to deposit sulphur on the surface, as was done by O'Brien et al. [35], since depositing sulphur will alter the surface. The activity of each composition was evaluated based on the potential defined by the onset of the SO_2 oxidation reaction. This potential was calculated using the intercept of two straight lines that bound the curve as described by Cooper & McGinn [29]. A catalyst composition that has a low onset potential in the short term may excel in application conditions, and this screening test was only designed to identify promising compositions. The catalyst ratio(s) that exhibit(s) promising activity will undergo future analysis on glassy carbon disk inserts employing a conventional three-electrode setup, which does not form part of the scope of this study.

Results and Discussion

Calibration of Sputtering Rate

To ensure control over catalyst thickness and composition, critical attention was paid to the calibration of the sputtering- or deposition rate. Calibration is enabled by employing a built-in retractable and computer-controlled quartz crystal microbalance (QCM). The QCM is positioned in the centre of the four magnetron guns (Fig. 1c) and allows for the in situ measurement of the sputtering rate expressed as nm/min based on the frequency change of the oscillator and well-known relationships. The sputtering rate is influenced by the DC power of the sputtering gun as well as the chamber pressure (Fig. 4). The direct relationship between the DC power of each gun and the corresponding sputtering rate was evaluated for each metal (Ti, Au, Pd, Pt), and a representative graph (Fig. 5) was constructed. The calibration lines (equations in Fig. 5) are then used to calculate the time of deposition for the various electrocatalysts at a specific power setting.

In addition, calibration curves were obtained for each metal at chamber pressures between 2 and 30 mTorr. A very good correlation (R^2 higher than 0.99) was found as long as the chamber pressure was kept between 2 and 12 mTorr. For higher chamber pressures, the sputtering rate was quite low and hence the errors due to reading of QCM values were

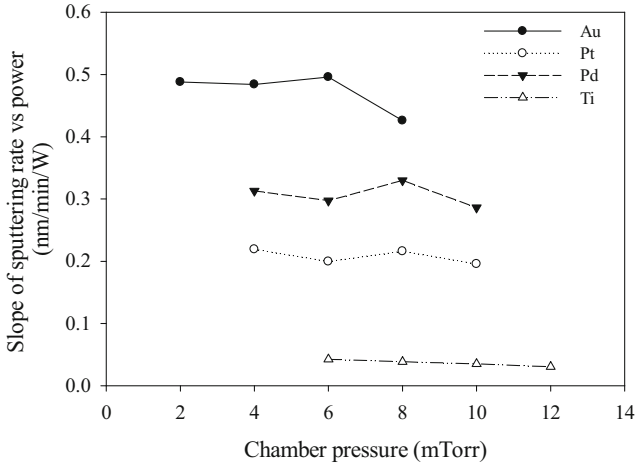

Fig. 4 The influence of the chamber pressure on the slope of the deposition rate versus DC power. The slope is obtained from calibration graphs similar to those in Fig. 5. Experimental conditions: vacuum base pressure, 5×10^{-7} Torr; argon gas flow rate, 0.015 L min^{-1}; and deposition time, 1 min

higher. Figure 4 shows the slope of the calibration graph obtained for different chamber pressures. As a global trend, it can be observed that the higher the chamber pressure, the lower the sputtering rate becomes. It was also observed that low chamber pressures, e.g. 2 and 4 mTorr, were not achievable for the deposition of Pt and Ti as the plasma could not be ignited. On the other hand, a chamber pressure higher than 10 mTorr was only achievable for the Ti target. As the chamber pressure is a crucial parameter for co-sputtering of two or more metals, it has to be convenient for all metals being sputtered. A pressure of 8 mTorr was subsequently chosen as a general pressure at which the deposition of any metal is possible. This combinatorial sputtering system is furthermore equipped with inlets for argon and oxygen, which could be used for reactive sputtering, with the flow rate of each sputtering gas that can be independently varied. In the case when only argon is used, as is the case for this study, the flow rate should not influence the sputtering rate. This was confirmed for the sputtering of Ti at a fixed chamber pressure and different DC powers of the magnetron gun (Fig. 6). As expected, no variation of the sputtering rate was observed with a change in the flow of argon, which confirms the proper functioning of the combinatorial sputtering setup.

Characterisation of Sputtered Films by Scanning Electron Microscopy

In order to investigate the morphology and stoichiometry of the sputtered thin films, SEM and EDX were conducted employing representative mapping of the co-deposited thin film electrocatalysts as a means of revealing the distribution of the Pt and Pd metals. As an example, Pt_3Pd_2 is shown in Fig. 7.

In general, the metals are seen to be homogeneously distributed as is expected from co-deposition, and as a result, the bulk composition is representative of the surface composition. To investigate the calibration (see the "Calibration of Sputtering Rate" section) of the PVD, the sputtered ratios were investigated by EDX analysis (Table 3). The results obtained from EDX deviated from the expected calibrated values in that the thin films were Pd deficient, with the $PtPd_9$ exhibiting a large standard deviation (STDV, obtained from three different positions on the wafer). A similar observation was made by Cooper et al. who sputtered PtRu combinations for methanol oxidation and found their thin films to be Ru

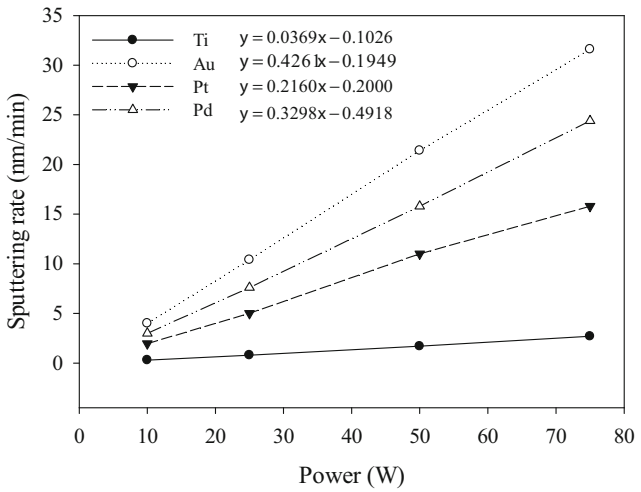

Fig. 5 A calibration curve for deposition rate versus power. Conditions: vacuum base pressure, 5×10^{-7} Torr; argon gas flow rate, 0.015 L min^{-1}; chamber pressure, 8 mTorr

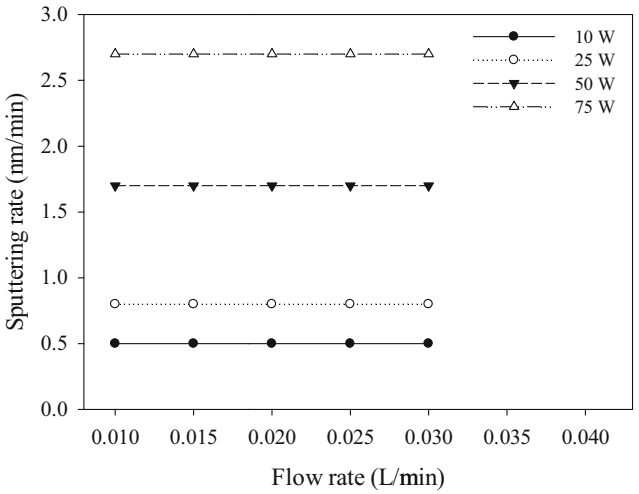

Fig. 6 The influence of the Ar flow rate on the final thickness of a Ti film for different values of the magnetron power. Experimental conditions: vacuum base pressure, 5×10^{-7} Torr; chamber pressure, 8 mTorr; deposition time, 1 min

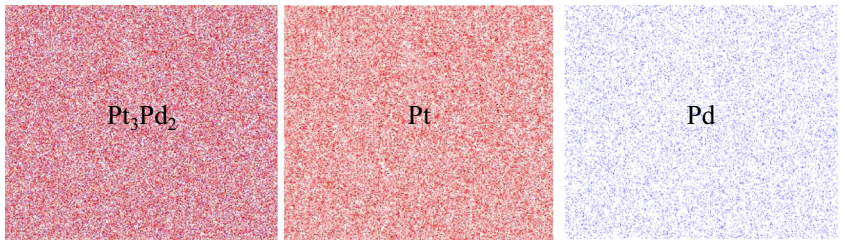

Fig. 7 Elemental mapping of as-deposited Pt_3Pd_2 electrocatalyst

deficient [36]. A similar trend is observed in that both Pd and Ru have a lower density than Pt, and in each case, it is the metal with the lower density that is deficient in the sputtered thin film. This clearly illustrates that for sputtered thin films, each composition has to be measured independently by a secondary method to obtain true compositional values.

SEM analysis was also conducted on a cross section of the pin pad to measure the thickness of the sputtered circuit layer (Fig. 8). This was done subsequent to electrochemical testing as SEM analysis requires cutting of the wafer. The thickness of the layer as measured by SEM analysis was 105.375 nm and is in accordance with our calibrated values.

Electrochemical Activity for SO_2 Oxidation

To validate the repeatability of the fabrication process of a sputtered electronic circuit, two wafers were fabricated employing the exact same steps and parameters. These two wafers, containing the exact same set of electrocatalysts, were independently electrochemically tested and compared for the electro-oxidation of aqueous SO_2. Each wafer contained three of each electrocatalyst sputtered on different positions in order to investigate the potential influence that different positions might have on the electric signal. The fabrication of two wafers furthermore served to investigate repeatability between wafers.

Onset potential is considered by many authors [29, 37–39] to be one of the indicators for catalytic activity of a catalyst and whether a catalyst is effective for the reaction of interest. With the onset potential of Pt being the target potential for the electro-oxidation of aqueous SO_2, every library contained several Pt sputtered catalysts as reference points. From a plot of the average onset potentials for Au, Pt, Pd and Pt_xPd_y electrocatalysts (Fig. 9), it is clear that Au exhibited the worst performance, followed by Pd, Pt, and the Pt_xPd_y combinations all being in close proximity of Pt. The average onset potential of 0.598±0.011 V (SHE) for Pt, for the electro-oxidation of SO_2, agrees well with literature [2, 35], which serves as the first confirmation that the data generated by the experimental system is acceptable. This average value is calculated from the average of the two wafers for a set of three electrocatalysts on each wafer. An example of composing this average onset potential value and standard deviation (STDV) is given in Table 4. The overall average difference between the two wafers for all the electrocatalysts was calculated as 0.728 %, which is very good taking into account all the steps required for fabricating a wafer, sputtering the thin film catalysts onto the wafer and conducting electrochemical screening.

Table 3 Atomic ratio (%) of sputtered Pt_xPd_y thin film electrocatalysts

Catalyst (%)		Measured atomic %		
Pt	Pd	Pt	Pd	STDV
80	20	83.137	16.863	1.487
60	40	67.920	32.080	0.626
40	60	49.083	50.917	0.100
20	80	31.928	68.137	1.888
10	90	25.635	74.365	5.904

STDV standard deviation

The electrocatalysts that exhibited promising activity are Pt_3Pd_2, Pt_2Pd_3 and $PtPd_4$, indicating that the addition of Pd results in a slight improvement as their onset potentials are slightly lower than that of pure Pt (Fig. 9). With a decrease in Pt content, it is clear that no trend is observed with regard to the change in onset potential. Pt_2Pd_3 exhibits the highest onset potential of the three promising electrocatalysts (see rectangular box in Fig. 9), while Pt_3Pd_2 and $PtPd_4$ resulted in the same lowest average onset potential, making them potential alternative catalysts compared to Pt. The Pt_3Pd_2 catalyst contains ~32 % less Pt, while the $PtPd_4$ catalyst contains ~68 % less Pt than the pure Pt catalyst (based on EDX analysis). Possible reasons for deviation in the onset potential values may be that Pt is sensitive to minute amounts of inorganic and organic contaminants that may remain on the surface due to the photolithographic processing that the electrocatalysts are exposed to [29, 40] and also the deviation in composition measured by EDX. The combinations tested have two commonalities, i.e. the fact that they catalyse the oxidation of SO_2 having a lower onset potential as well as the undeniable fact that they all use less Pt to achieve this.

Current density, as another characteristic indicator of catalyst activity, was not employed during this investigation for, to make a worthy comparison using current density, the real active surface area is required. The real active surface area of a pure Pt surface is mostly determined by examining and integrating the monolayer hydrogen adsorption area after

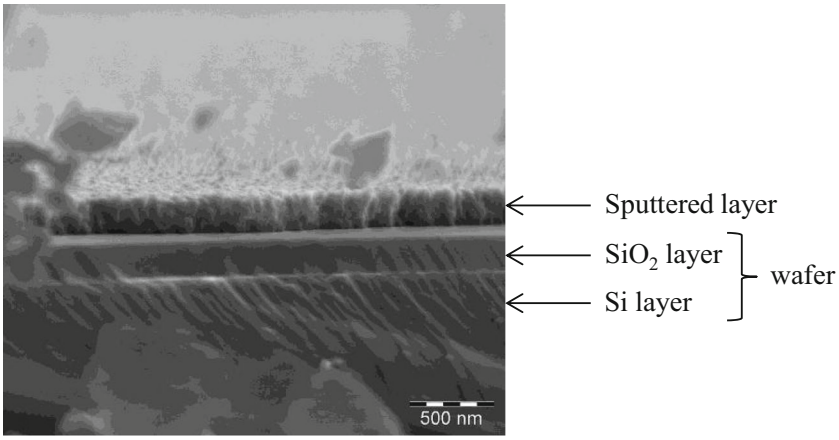

Fig. 8 Cross view of the Si-SiO_2-TiAu layers of a wafer

consecutive potential sweeps [41–43]. The combinatorial approach investigated here includes varying catalysts like Au and Pd, which do not contain any Pt at all. Hence, the method of oxygen adsorption from solution should be used for the estimation of real surface area as this method is common to all the metals under investigation [43]. Multiple runs to a set of upper potential limits, at which oxygen is chemisorbed in a monoatomic layer with a one-to-one correspondence with the surface metal atoms, have to be conducted [44]. This requires the catalyst surface to be identical at the commencement of each run, and since our various catalysts are positioned on a wafer which cannot undergo physical polishing/cleaning, they will have to undergo some sort of electrochemical cleaning and/or other means of obtaining a repeatable surface. Furthermore, for the electro-oxidation of aqueous SO_2, sulphur as well as other intermediate oxidation products has variable adsorption/binding strengths on the different metals and metal combinations, which will affect the specific technique that is employed to determine the real active surface area [32]. Whichever method is employed to determine the real active surface area, all have their advantages and limitations [41]. In this instance, after weighing the advantages and limitations of using oxygen adsorption from solution as a means to determine the real active surface area of the variety of catalysts prepared employing our combinatorial setup, it was decided not to disregard the method, but that it deserves a dedicated investigation [29]. One could use geometric area, as stated by Cooper & McGinn [34], but employing the real active surface area is preferred as it is sure to differ from the geometric area for different catalyst compositions. Hence, for this investigation, only onset potential was employed as a means to quickly identify promising compositions from a catalyst library for the electro-oxidation of aqueous SO_2 [34].

In order to clearly identify a possible alternative catalyst compared to pure Pt, further in-depth investigations have to be conducted on the Pt_3Pd_2 and $PtPd_4$ catalysts. This will entail sputtering these combinations onto GCs to (i) investigate and improve catalyst stability, (ii) conduct real active surface area measurements so as to calculate and compare current densities, and (iii) conduct linear polarisation scans at different temperatures in order to calculate activation energy.

Table 4 Example of composing the average onset potential value and standard deviation for Pt

Pt	Wafer 1	Wafer 2
Onset potential (V, SHE)	0.609	0.606
	0.603	0.600
	0.581	0.591
Pad-to-pad reproducibility	0.598±0.015	0.599±0.008
Wafer-to-wafer reproducibility	0.598±0.011	

Conclusions

A combinatorial method for the synthesis and electrochemical screening of novel functional materials has been described. Pure Au, Pt, Pd and bimetallic Pt_xPd_y electrocatalysts were

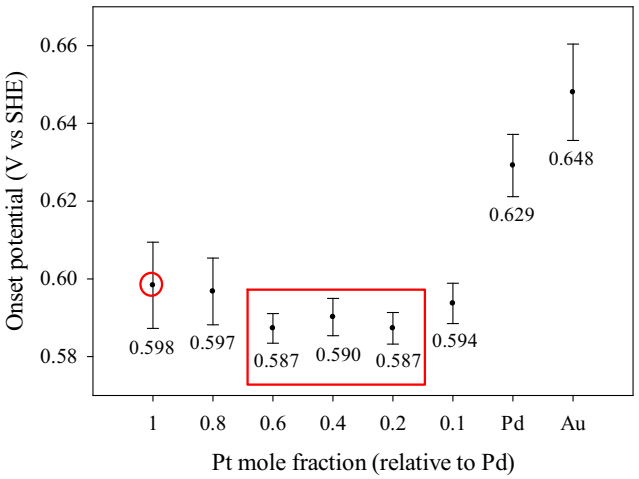

Fig. 9 Average onset potentials for Au, Pd, Pt and Pt_xPd_y electrocatalysts on a SiO_2 wafer. Conditions: 1 mol L^{-1} H_2SO_4, 100 mmol L^{-1} SO_2, 25 °C, 10 mV s^{-1}

sputtered onto a silica wafer and screened for activity towards the electro-oxidation of aqueous SO_2, employing onset potential as the screening criterion. On the wafer, three Pt_xPd_y bimetallic combinations exhibited satisfactory performance (compared to pure Pt) with the best compositions being Pt_3Pd_2 and $PtPd_4$. Both these combinations exhibited the same lower onset potential of 0.587±0.004 V, SHE compared to that of pure Pt (0.598±0.011 V, SHE). It has been shown that Pt content can be significantly reduced, through the development of a bimetallic electrocatalyst for the electro-oxidation of aqueous SO_2, whilst not sacrificing catalytic activity (based on onset potential).

Acknowledgments The financial assistance of the National Research Foundation (NRF) towards this research is hereby acknowledged. Opinions expressed and conclusions arrived at are those of the authors and are not necessarily to be attributed to the NRF. The assistance of Dr. L. Tiedt with SEM and EDX is gratefully acknowledged.

References

1. W.A. Summer, M.B. Gorensek, M.R. Buckner, The hybrid sulfur cycle for nuclear hydrogen production, Doc No. WSRC-MS-2005-00509, Report No. OSTI ID: 881467, 8 September, (2005)
2. J.A. O`Brien, J.T. Hinkely, S.W. Donne, J. Electrochem. Soc. **159**, F585 (2012)
3. H. Colon-Mercado, M. Elvington, D. Hobbs, Close-out report for HyS electrolyzer component development work at Savannah River National Laboratory, Report No. SRS SRNL-STI-2010-00019, (2010)
4. L. Xue, P. Zhang, S. Chen, L. Wang, Int. J. Hydrog. Energy **39**, 14196 (2014)
5. R. C. Weast, *CRC Handbook of Chemistry and Physics*, 70th edn. (CRC Press Inc, Boca Raton, Florida, 1989-1990)
6. B.D. Struck, R. Junginger, D. Boltersdorf, J. Gehrmann, Int. J. Hydrog. Energy **5**, 487 (1980)
7. R.J. Kriek, J.P. van Ravenswaay, M. Potgieter, A. Calitz, V. Lates, M.E. Bjorketun, S. Siahrostami, J. Rossmeisl, J. S. Afr. Inst. Min. Metall. **113**, 593 (2013)
8. M.B. Gorensek, W.A. Summer, C.O. Bolthrunis, E.J. Lahoda, D.T. Allen, R. Greyvenstein, Hybrid Sulfur Process Reference Design and Cost Analysis - Final Report SRNL-L1200-2008-00002. Rev 1, (2009)
9. K. Wiesener, Electrochim. Acta **18**, 185 (1973)
10. P. Lu, R. Ammon, J. Electrochem. Soc. **127**, 2610 (1980)
11. H.R. Colon-Mercado, D.T. Hobbs, Electrochem. Commun. **9**, 2649 (2007)
12. J. Loskyll, K. Stoewe, W.F. Maier, Sci. Technol. Adv. Mater. **12**, 0541011 (2011)
13. P. Strasser, Q. Fan, M. Devenney, W.H. Weinberg, J. Phys. Chem. B **107**, 11013 (2003)
14. E.S. Smotkin, J. Jiang, A. Nayar, R. Liu, Appl. Surf. Sci. **252**, 2573 (2006)
15. A.D. Spong, G. Vitins, S. Guerin, B.E. Hayden, J. Power Sources **119–121**, 778 (2003)
16. T. Gebhardt, D. Music, T. Takahashi, J.M. Schneider, Thin Solid Films **520**, 5491 (2012)
17. J.J. Hanak, J. Mater. Sci. **5**, 964 (1970)
18. X.D. Xiang, X. Sun, G. Briceno, Y. Lou, K. Wang, H. Chang, W.G. Wallace-Freedman, S. Chen, P.G. Scultz, Science **268**, 1738 (1995)
19. X.D. Xiang, Annu. Rev. Mater. Sci. **29**, 149 (1999)
20. M. Black, J. Cooper, P. McGinn, Chem. Eng. Sci. **59**, 4839 (2004)
21. S. Miertus, G. Fassina, *Combinatorial chemistry and technology* (Marcel Dekker, New York, 1999)
22. R.W. Cahn, Nature **410**, 643 (2001)
23. R.B. van Dover, L.F. Schneemeyer, R.M. Fleming, Nature **392**, 162 (1998)
24. Y. Matsumoto, M. Murakami, Z. Jin, A. Ohtomo, M. Lippmaa, M. Kawasaki, H. Koinuma, Jpn. J. Appl. Phys. **38**, L603 (1999)
25. H. Chang, I. Takeuchi, X.D. Xiang, App. Phys. Lett. **74**, 1165 (1999)
26. W.F. Maier, K. Stowe, S. Sieg, Angew. Chem. Int. Ed. **46**, 6016 (2007)
27. E. Reddington, A. Sapienza, B. Gurau, R. Viswanathan, S. Saragapani, E.S. Smotkin, T.E. Mallouk, Science **280**, 1735 (1998)
28. C.K. Kjartansdottir, L.P. Nielsen, P. Moller, Int. J. Hydrog. Energy **38**, 8221 (2013)
29. J.S. Cooper, P.J. McGinn, Appl. Surf. Sci. **254**, 662 (2007)
30. L. Wang, P. Zhang, S. Chen, J. Xu, Nucl. Eng. Des. **271**, 60 (2014)
31. P.W.T. Lu, R.L. Ammon, Int. J. Hydrog. Energy **7**, 563 (1982)
32. R.J. Kriek, J. Rossmeisl, S. Siahrostami, M.E. Bjorketun, Phys. Chem. Chem. Phys. **16**, 9572 (2014)
33. C.J. Warren, R.C. Haushalter, L. Matsiev, Combinatorial electrochemical deposition and testing system, vol. US 6756109 B2 (Symyx Technologies, Inc., 2004)
34. J.S. Cooper, P.J. McGinn, J. Power Sources **163**, 330 (2006)
35. J.A. O'Brien, J.T. Hinkley, S.W. Donne, J. Electrochem. Soc. **157**, F111 (2010)
36. J.S. Cooper, G. Zhang, P.J. McGinn, Rev. Sci. Instrum. **76**, 062221 (2005)
37. C. Song, J. Zhang, in *PEM Fuel Cell Electrocatalysts and Catalyst Layers*, ed. by J. Zhang, (Springer-Verlag London Limited, 2008), p. 97
38. S. Jayaraman, A.C. Hillier, J. Comb. Chem. **6**, 27 (2004)
39. M.U. Kleinke, M. Knobel, L.O. Bonugli, O. Teschke, Int. J. Hydrog. Energy **22**, 759 (1997)
40. B.D. McNicol, R. Miles, R.T. Short, Electrochim. Acta **28**, 1285 (1983)
41. S. Trasatti, O.A. Petrii, Pure Appl. Chem. **63**, 1285 (1991)
42. T. Bieger, D.A.J. Rand, R. Woods, J. Electroanal. Chem. **29**, 269 (1971)
43. R.P. Simprag, B.E. Conway, Electrochim. Acta **43**, 3045 (1998)
44. L. Fang, Q. Tao, M. Li, L. Liao, D. Chen, Y. Chen, Chin. J. Chem. Phys. **23**, 543 (2010)